Supporting Information

Wall Density-Controlled Thermal Conductive and Mechanical Properties of Three-Dimensional Vertically Aligned Boron Nitride Network-Based Polymeric Composites

Fang Jiang[1, 2], Na Song[2], Runhai Ouyang[3] and Peng Ding[,1,2]*

[1]School of Materials Science and Engineering, Shanghai University, 99 Shangda Road, Shanghai 200444, PR China

[2]Research Center of Nanoscience and Nanotechnology, Shanghai University, 99 Shangda Road, Shanghai 200444, PR China

[3]Materials Genome Institute, Shanghai University, 333 Nanchen Road, Shanghai 200444, PR China

* Corresponding Author, Tel&Fax: +86-2166134726, Email: dingpeng@shu.edu.cn (P. Ding)

Contents:

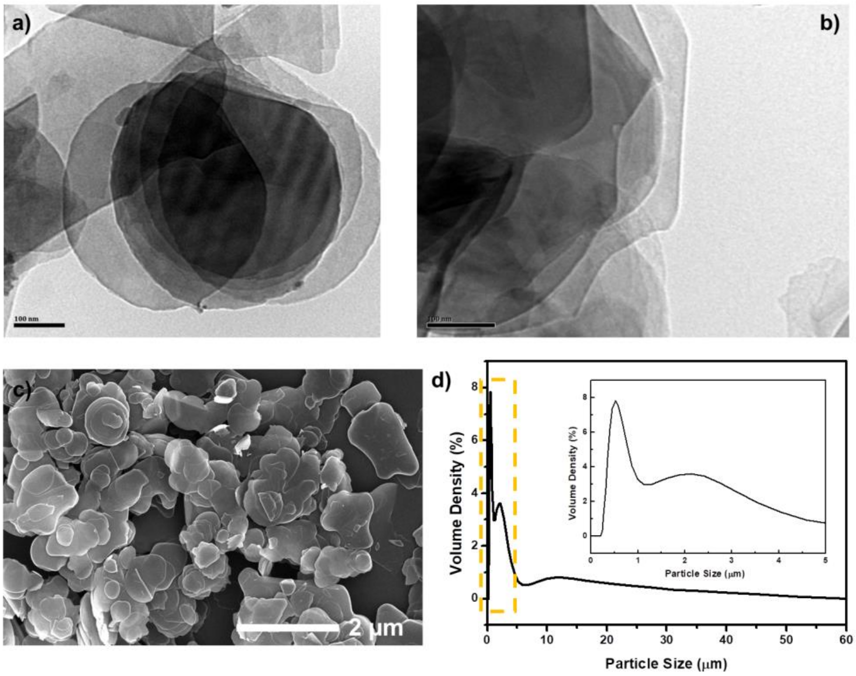

Figure S1. a, b) TEM c) SEM images of FBN. d) FBN size distribution measurement.

Table S1. BN loading in PBNF composites.

	PVA (g)	BN (g)	BN loading in composites (vol%)
PBNF1	0.03	0.1	1.2
PBNF2	0.03	0.2	3.0
PBNF3	0.03	0.3	4.2
PBNF4	0.03	0.4	4.5
PBNF5	0.03	0.5	6.9
PBNF6	0.03	0.6	7.3
PBNF7	0.03	0.7	8.1

Table S2. Conversion of mass fraction into volume fraction.

		BNNSs loading in composites (wt%)	BNNS loading in composites (vol%)
PBNF1	PBN1	2.1	1.2
PBNF2	PBN2	5.2	3.0
PBNF3	PBN3	7.3	4.2
PBNF4	PBN4	7.7	4.5
PBNF5	PBN5	11.7	6.9
PBNF6	PBN6	12.4	7.3
PBNF7	PBN7	13.6	8.1

Calculation method:

Density at standard conditions: $\rho_1=\rho_{BN}=2.27$ g/cm^3 $\rho_2=\rho_{PVA}=\rho_{PEG}=1.27$ g/cm^3

The volume fraction of BN filler is calculated through the equation:

$$BN_{\mathrm{vol\%}} = \frac{wt\%/\rho_1}{wt\%/\rho_1 + (1-wt\%)/\rho_2}$$

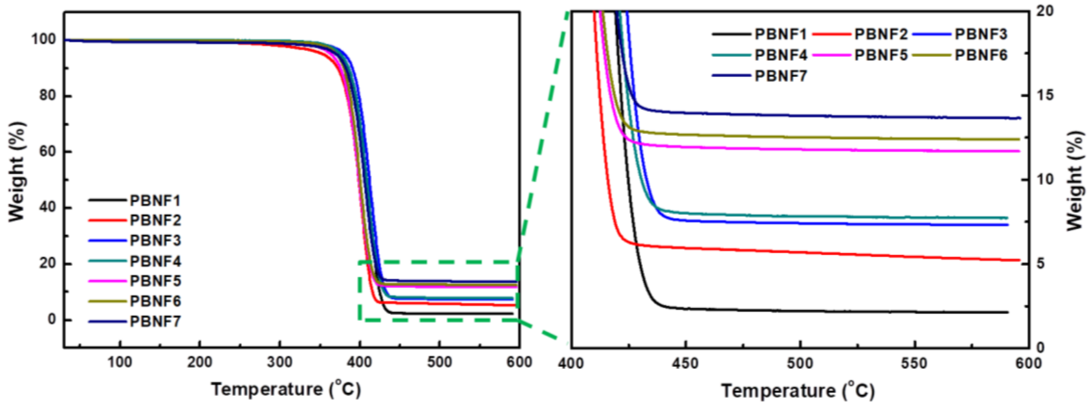

Figure S2. TGA curves of PBNF1, PBNF2, PBNF3, PBNF4, PBNF5, PBNF6, PBNF7 composites.

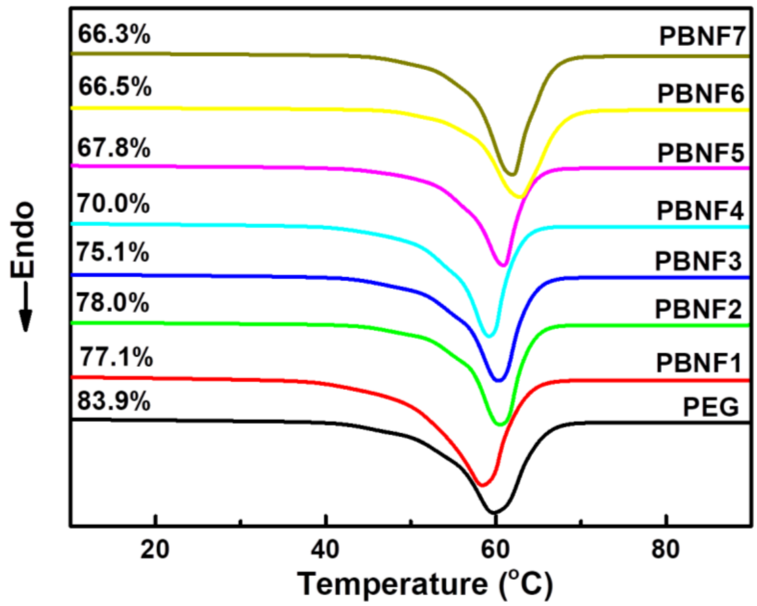

Figure S3. DSC curves of PEG and PBNF composites with different wall density.

As shown in Figure S3, with the increasing of BN loading, the crystallinity decreases according. This is mainly because the existence of BN restricted the free movement of PEG chains.[1-3]

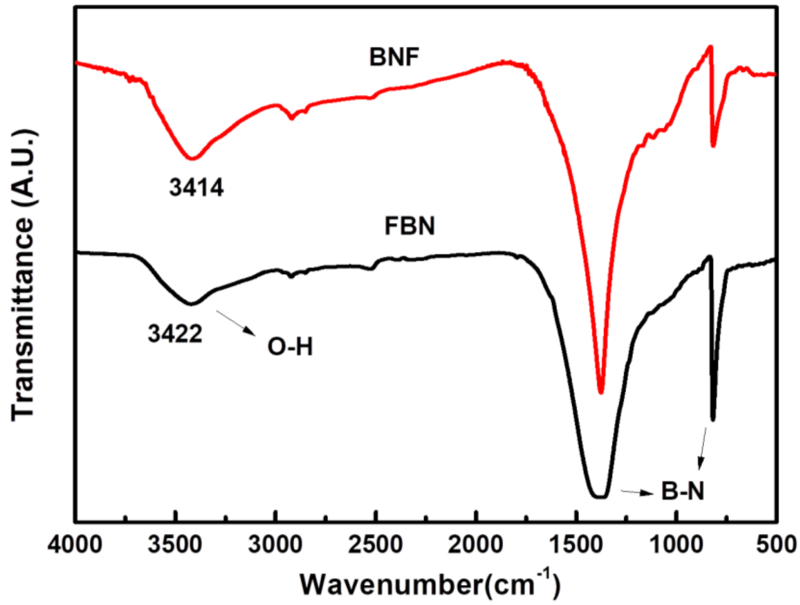

Figure S4. FTIR spectra of FBN and BNF scaffold.

As can be seen in Figure S4, two typical absorption peaks at 1393 and 806 cm^{-1} due to the stretching and deformation vibrations of B-N bonds, respectively, are observed in the FTIR spectra of FBN and BNF scaffold.[4] A peak at 3422 cm^{-1} attributed to the successful hydroxylation of the BN, which is ascribed to O-H stretching vibrations.[5] A peak shift of the hydroxyl stretching band occurred in BNF owing to the formation of hydrogen bond.[1]

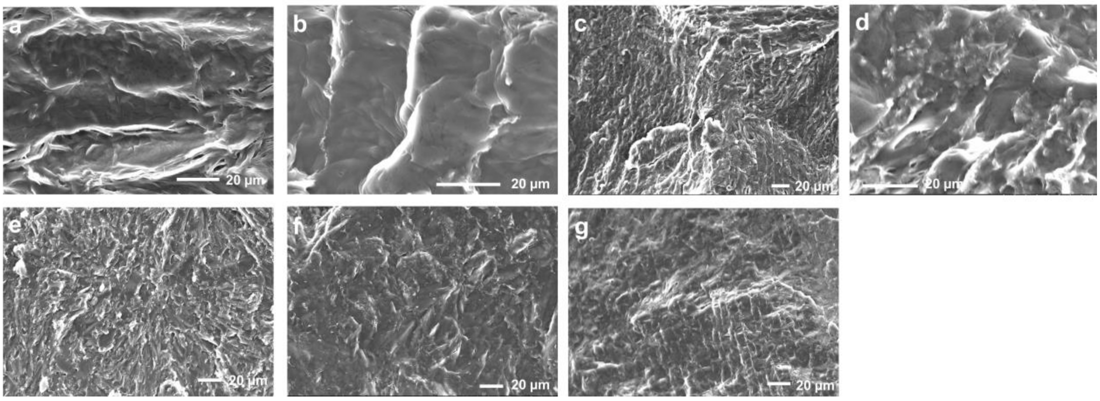

Figure S5. SEM images of a) PBNF1, b) PBNF2, c) PBNF3, d) PBNF4, e) PBNF5, f) PBNF6 and g) PBNF7 composites.

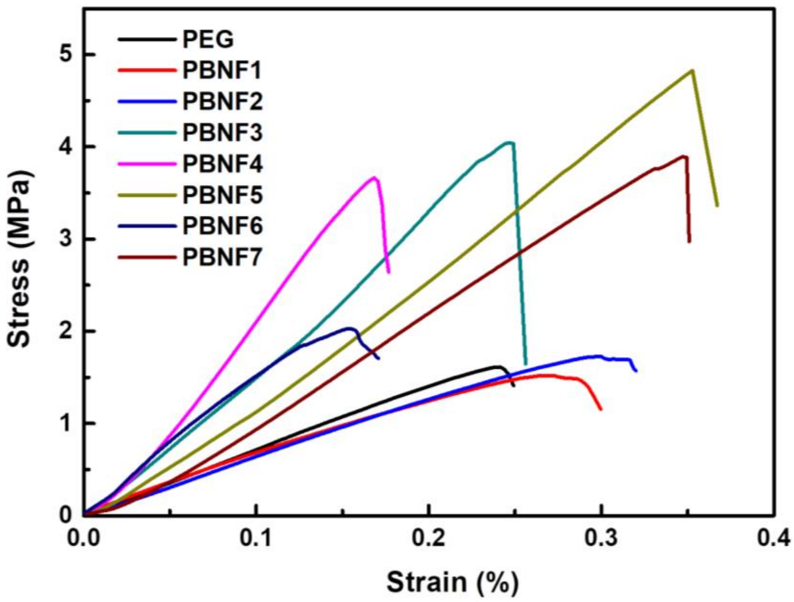

Figure S6. Strain-stress curves of PEG and PBNF composites with different wall density.

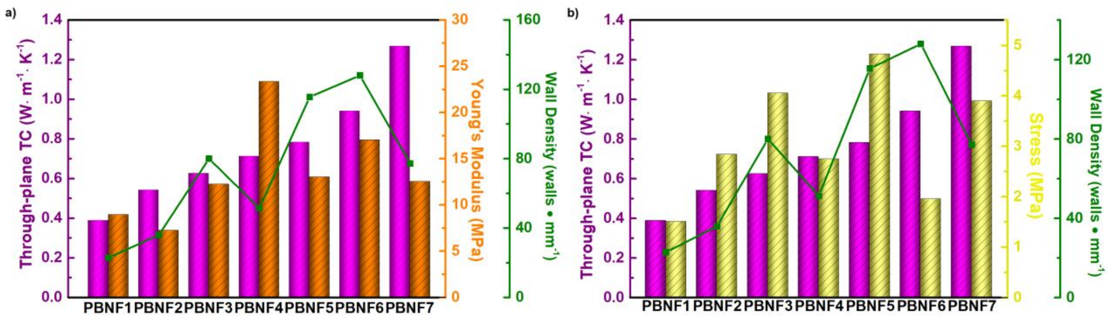

Figure S7. The relationship between through-plane TC, a) Young's modulus b) stress and wall density.

SISSO calculation parameters. SISSO is a data-driven method based on compressed-sensing for identifying interpretable models even with small datasets. A feature space is firstly constructed by recursively transforming input variables into complex features via various mathematical operations, and then the best model is identified by sparsifying the linear model of the target property expanded in the feature space. The operators used for feature construction is: +, -, *, /, exp, exp(-), ^-1, ^2, ^3, sqrt, cbrt, log, | - |. Since the dataset are very small (7 data for each machine learning), we restrict the model to the lowest dimension of 1D (one coefficient in addition to the intercept in the linear model). Feature complexity (the maximal number of operators in a feature) was increased from low to high, and the selected model is the balance between training accuracy and the complexity. The best feature complexity was found at 2, 4, and 1 for y_c, y_m, and y_d, respectively. The used primary features (input variables) are wt_{PVA} and wt_{BN} for learning both y_c, and y_d. For learning y_m, we found wt_{PVA} and wt_{BN} did not yield good results, but with the inclusion of y_c it was greatly improved.

Table S3. The training data for SISSO model building.

sample	y_c (W m^{-1} K^{-1})	y_d (walls mm^{-1})	y_m (MPa)	wt_{PVA} (wt%)	wt_{BN} (wt%)
PBNF1	0.38644	22.9	8.9	0.63	2.1
PBNF2	0.53997	36	7.2	0.78	5.2
PBNF3	0.62454	80	12.2	0.73	7.3
PBNF4	0.71019	51.4	23.3	0.5775	7.7
PBNF5	0.78181	115.6	13	0.702	11.7
PBNF6	0.93926	128	17	0.62	12.4
PBNF7	1.26699	77.2	12.5	0.582857	13.6

y_c represents the experimental observed thermal conductivity; y_d represents the experimental observed wall density; y_m represents the experimental observed Young's modulus; wt_{PVA} and wt_{BN} represent the weight ratio in the corresponding PBNF composites.

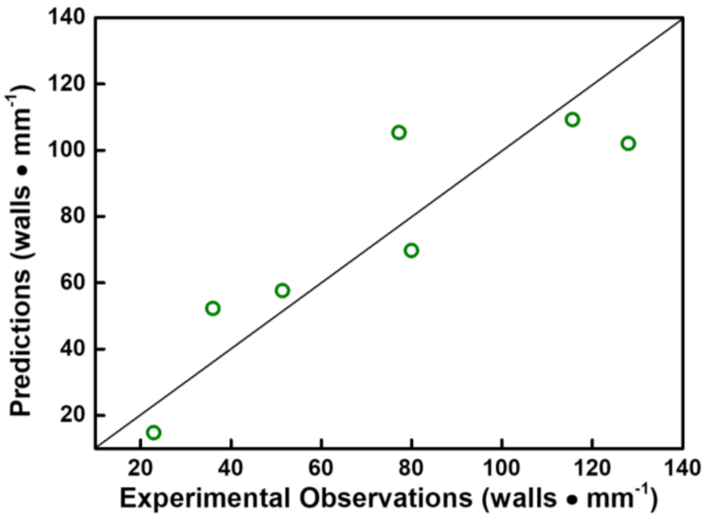

Figure S8. SISSO machine learning of optimal analytical expression for wall density of BNF scaffolds, the circle represent for the comparison of wall density between the model $y_d = -3.351 + 13.713 \times wt_{BN} \times wt_{PVA}$ and the experimental observation values.

The description of the model $y_d = -3.351 + 13.713 \times wt_{BN} \times wt_{PVA}$ is not very well. This is mainly because the wall density is not only related to the component content in the BNF scaffolds, but also affected by freeze-drying process. The parameter of freeze-drying, the temperature of the cold source during freezing, freezing rate during the freezing process, the content of different components, the morphology of filler would all affect the morphology of the fabricated scaffold.[6-10] Therefore, some deviation will occur in the equation.

References

1. Kim, G. H.; Lee, D.; Shanker, A.; Shao, L.; Kwon, M. S.; Gidley, D.; Kim, J.; Pipe, K. P. High Thermal Conductivity in Amorphous Polymer Blends by Engineered Interchain Interactions. *Nat. Mater.* **2015,** *14*, 3, 295-300.
2. Ding, P.; Zhuang, N.; Cui, X.; Shi, L.; Song, N.; Tang, S. Enhanced thermal conductive property of polyamide composites by low mass fraction of covalently grafted graphene nanoribbons. *J. Mater. Chem. C* **2015,** *3*, 42, 10990-10997.
3. Song, P. A.; Xu, Z. G.; Guo, Q. P. Bioinspired Strategy to Reinforce PVA with Improved Toughness and Thermal Properties via Hydrogen-Bond Self-Assembly. *ACS Macro Lett.* **2013,** *2*, 12, 1100-1104.
4. Yu, B.; Xing, W.; Guo, W.; Qiu, S.; Wang, X.; Lo, S.; Hu, Y. Thermal exfoliation of hexagonal boron nitride for effective enhancements on thermal stability, flame retardancy and smoke suppression of epoxy resin nanocomposites via sol–gel process. *J. Mater. Chem. A* **2016,** *4*, 19, 7330-7340.
5. Sainsbury, T.; Satti, A.; May, P.; Wang, Z.; McGovern, I.; Gun'ko, Y. K.; Coleman, J. Oxygen radical functionalization of boron nitride nanosheets. *J. Am. Chem. Soc.* **2012,** *134*, 45, 18758-71.
6. Li, X. H.; Liu, P. F.; Li, X. F.; An, F.; Min, P.; Liao, K. N.; Yu, Z. Z. Vertically Aligned, Ultralight and Highly Compressive All-Graphitized Graphene Aerogels for Highly Thermally Conductive Polymer Composites. *Carbon* **2018,** *140*, 624-633.
7. Yang, M.; Zhao, N. F.; Cui, Y.; Gao, W. W.; Zhao, Q.; Gao, C.; Bai, H.; Xie, T. Biomimetic Architectured Graphene Aerogel with Exceptional Strength and Resilience. *ACS Nano* **2017,** *11*, 7, 6817-6824.
8. Zhao, N. F.; Yang, M.; Zhao, Q.; Gao, W. W.; Xie, T.; Bai, H. Superstretchable Nacre-Mimetic Graphene/Poly(vinyl alcohol) Composite Film Based on Interfacial Architectural Engineering. *ACS Nano* **2017,** *11*, 5, 4777-4784.
9. Han, J. K.; Du, G. L.; Gao, W. W.; Bai, H. An Anisotropically High Thermal Conductive Boron Nitride/Epoxy Composite Based on Nacre-Mimetic 3D Network. *Adv. Funct. Mater.* **2019,** *29*, 13, 1900412.
10. Bai, H.; Chen, Y.; Delattre, B.; Tomsia, A. P.; Ritchie, R. O. Bioinspired Large-Scale Aligned Porous Materials Assembled with Dual Temperature Gradients. *Sci. Adv.* **2015,** *1*, 11, No.8.